Scattering of electrons by alkali-halide molecules: LiBr and CsCl

L. Vušković,* M. Zuo, G. F. Shen,† B. Stumpf,‡ and B. Bederson
Department of Physics, New York University, New York, New York 10003
(Received 12 December 1988)

We have investigated small-angle electron scattering by highly polar molecules. Recoil experiments are performed at 5 and 20 eV for electrons scattered by LiBr and CsCl, within the shadow of the unscattered molecular beam. Low-angular-range scattering described by the Born approximation for rotating dipoles, combined with different theories for intermediate- and high-angle scattering, are compared with our results. Evaluated total scattering cross sections as well as momentum-transfer and viscosity cross sections are given. A general two-dimensional analysis of the recoil experiment is presented.

I. INTRODUCTION

The study of electron scattering by molecules with permanent electric dipole moments has been an active field of collision physics for over five decades. From a practical point of view, such collisions play dominant roles in a variety of transport phenomena, including seeded thermionic conversion and magnetohydrodynamic devices. Also, the large cross sections for electron scattering by highly polar molecules make them attractive as candidates for electronically pumped lasers.

The first significant theoretical development in this field was Massey's observation[1] that the Born approximation will hold for electron–polar-molecule differential cross sections at all electron energies, assuming that the long-range monopole-dipole interaction dominates the collision process. While the fixed-dipole approximation for this interaction diverges at small angles, the more realistic rotating-point-dipole approximation yields both a convergent and analytic result. The cross sections are very strongly peaked in the forward direction and are dominated by the electronically and vibrationally elastic and rotationally inelastic process with $|\Delta j| = 1$.

While this long-range interaction must of course dominate the interaction at sufficiently large-impact parameters, the question of how the higher-order multipole moments, and indeed the full electron-molecule interaction, contribute to small-angle scattering remains open. A variety of approaches, both semiclassical and fully quantum mechanical, have been employed in recent years in connection with this problem. We refer the reader to review articles by Norcross and Collins,[2] Itikawa,[3] and Lane[4] for discussions of recent experimental and theoretical developments. After the appearance of the last review paper,[2] Padial *et al.*[5] studied vibrational excitations in quasielastic scattering of electrons on HCl, which possesses an electron dipole moment of 1.1 D, in the thermal energy range in a close-coupling calculation. Padial and Norcross[6] also reported on simultaneous rotational and vibrational excitation cross sections for the same molecule and energy range, using an adiabatic approximation based on a molecule multipole expansion.

Dissociative attachment of electrons have been studied by Teillet-Billy and Guayacq[7] in the energy range 0–1 eV for HCl and DCl. They employ effective range theory,[8] which specifically includes the long-range polarization force and short-range forces. Vibrational excitation and dissociative electron-attachment cross sections for energies up to 5 eV for HCl and DCl have also been calculated by Domcke and Mundel,[9] using a nonadiabatic theory of near-threshold resonant electron-molecule scattering in the presence of a long-range potential.[10] Recently, Bijker and Amado[11] calculated rotational and vibrational excitation for the highly polar molecules LiF (6.33 D) and KI (10.82 D), using an algebraic eikonal approach based on an adiabatic, fixed nuclei approximation, for energies well above rotational and vibrational excitation energies. They combine an algebraic description of the molecular dynamics, the vibrion model, in the adiabatic limit with eikonal scattering methods and calculate elastic and inelastic scattering to excited rotational and vibrational states. In order to compare with experiment, they sum over final rotational states and average over initial ones.

The principal purpose of this present work is to explore experimentally the behavior of differential cross sections of highly polar (i.e., alkali-halide) molecules at low interaction energies and at a wide range of scattering angles, in order to study specifically the long-range parts of the electron–polar-molecule interaction, as well as the roles played by short-range forces even at small angles.

In dealing with experiment it is convenient to divide polar-molecule scattering into two categories. The first refers to polar molecules with electric dipole moments of the order of 1 D, and the second with so-called "highly polar" molecules with electric dipole moments in excess of, say, 6 D. A third category, of so-called "weakly polar" molecules, e.g., CO (0.11 D) will not be considered here. There are, generally speaking, significant experimental difficulties experienced in dealing with the highly polar category, compared to the polar one. The former can significantly affect surface potentials of electron optics elements, since they are generally condensables at room temperature. Unlike most polar molecules, they generally require relatively high temperatures to vaporize (700 to 1000 °C). As a consequence for this class of polar molecules it is not practical to obtain experimental absolute values by normalization of the measured electron

scattering intensity, such as in the flux-flow method,[12] using the electron-helium elastic differential cross section as a standard. The reliable determination of *absolute* cross sections for highly polar molecules remains one of the most challenging problems in electron-molecule collision physics.

The values of dipole moments of polar molecules are in the vicinity of the "critical dipole moment" $D_c = 1.625$ D, the minimum value required for a stationary dipole to bind an electron.[13] Numerous experiments were performed by Rohr and Linder[14,15] (HCl; HF, 1.8 D), Seng and Linder[16] (H_2O, 1.86 D), Rohr[17–19] (HBr, 0.8 D; H_2S, 0.98 D), Shon *et al.*[20] (OCS, 0.71 D), and Azria *et al.*[21,22] (HBr, HCl) to study differential cross sections for elastic scattering, vibrational and rotational excitation, and dissociative attachment. These are crossed-beam experiments employing conventional electron spectrometers[14,23] with a 127° cylindrical electrostatic selector in an electron gun and a detector operating in the energy range, close to the threshold. For dissociative attachment a magnetic momentum filter[24,25] is also used to separate electrons from the negative ions. These experiments performed with high-energy resolution (as low as 22 meV) provide detailed information concerning resonant structure in elastic and inelastic channels. However, it is difficult by this means to obtain absolute-cross-section values, these varying by up to a factor of 2 for various such determinations.[17]

The second group of experiments, devoted to highly polar molecules, concern themselves mainly with the alkali halides. In such experiments performed to date, so-called "potential scattering," rather than high-resolution excitation studies, have been the primary emphasis. Measurements have generally not been performed with energy resolution sufficient to distinguish separately rotational and vibrational states, and results are generally reported on the sum of elastic and thermally averaged rotational and vibrational excitations. Even so, crossed-beam measurements using 180° hemispherical electron guns and analyzers have been performed by Rudge *et al.*[26] (KI), Srivastava *et al.*[27] (HCN, 2.98 D), Vušković *et al.*[28] (LiF), and Vušković and Srivastava[29] (CsCl, 10.55 D). Relative, differential quasielastic cross sections have been measured in the energy range 5–60 eV. The most generally accepted procedure for normalization[29] is actually to theory, by normalizing at angles where several theoretical models agree. Since small-angle collisions (below 10°) have not been studied in these experiments, it is necessary to rely on theory to extrapolate the measurements to smaller angles (where, presumably, theory tends to be more reliable). As a consequence values of integrated cross sections, which heavily weigh small-angle collisions, are dominated by calculated rather than experimental data. The situation is somewhat different for momentum-transfer cross sections, which weigh larger-angle collisions more heavily and therefore as a consequence require a greater reliance on measured cross sections. Of course, in the angular range of overlap between theory and experiment, relative shapes as opposed to absolute values supply some guidance in comparison of theoretical models.

A series of experiments were performed at Columbia University by Stern and students in the early 1970s, using the molecular-beam recoil technique.[30] These included measurements by Slater *et al.*[31] (CsF, 7.88 D), Slater *et al.*[32] (KI), and Becker[33] (CsCl) of angular distributions of molecules which were recoil scattered in collisions with electrons. The kinematics of the electron-molecular momentum-transfer reaction enables one to infer the electron differential cross sections. Stern constructed model cross sections to compare with the recoil data. These were then employed to calculate integrated and momentum-transfer cross sections. This procedure, however, has been questioned by Collins and Norcross.[34] Jaduszliwer *et al.*[35,36] also used the recoil technique to measure "effective" absolute cross sections for scattering-out (from the forward direction) of alkali-halide molecules (CsBr, 10.82 D; RbBr, 10.36 D; RbCl, 10.51 D; CsCl; KI) by electrons in the energy range of 3–22.5 eV. (It is a characteristic of the recoil method that absolute cross sections can be obtained without knowledge of the atomic or molecular-beam density.[30]) These data were presented as effective cross sections because of the special problem associated with small-angle scattering by highly polar molecules. Apparatus functions which explicitly presented angular "form factors" were also given to allow for a direct comparison with differential cross sections obtained from theory.

In the present work we present additional recoil-type measurements at 5 and 20 eV for electrons scattered by LiBr (7.23 D) and CsCl. The emphasis in this work is in a further effort to account for scattering at all angles, including the very small angles which are not normally observable in elastic collisions. Thus measurements were made primarily within the shadow of the unscattered molecular beam where small-angle collisions have a very important contribution. In order to understand how the measured signal is related to the scattering into and out of the detector we developed an analytic model that fully describes the scattering process in the presence of an unscattered beam. The analysis is general in the sense that it would apply to either the electron or the molecular beam, although the specific relations developed here apply primarily to the latter case. In the analysis we transform a two-dimensional molecular-deflection profile resulting from a crossed-beam interaction into a unique set of scattering cross sections.

II. RECOIL ANALYSIS

Our aim here is to present an analysis that describes the scattering process in a recoil experiment. To be more specific, the purpose of this analysis is to transform a two-dimensional atomic deflection profile resulting from an atomic (molecular) species crossfired by an electron beam with observation made on the scattered atoms to infer a unique set of scattering cross sections.[37,38]

Schematic diagrams of atomic recoil and electron scattering angles, as well as the relations between them, are given in Ref. 39. Here we recall some of the pertinent results. We denote coordinates in the interaction region by x',y',z', and in the detector plane by x,y,z, as indicat-

ed in Fig. 1. The atom beam is propagating along the y (or y') axis (momentum magnitude MV) and the electron beam along the z' axis (momentum magnitude mv). Recoil atoms are measured in the (x,z) plane, which is a distance L from the interaction volume. The quantities y,y' are related by $y=y'+L$.

We first derive results assuming both monoenergetic electrons and atoms. Under the condition $mv \ll MV$, the x,z coordinates[39] for elastic scattering are

$$x=\alpha L \sin\theta \sin\phi, \quad z=\alpha L(1-\cos\theta) , \tag{1}$$

where θ,ϕ are electron polar and azimuthal scattering angles, respectively, and $\alpha=mv/MV$. For inelastic scattering

$$x=\beta_k L \sin\theta \sin\phi, \quad z=L(\alpha-\beta_k \cos\theta) , \tag{2}$$

where $\beta_k=mv^k/MV$ and v^k is the electron velocity after the collision (the change of V is negligible). The state of the atom after the collision is indicated by subscript k, and here we assume that the atom was initially in the ground state.

Figure 1, referring to the right side, shows the (x,z) plane where the atom-beam measurements are made. The atom-beam cross sectional area gh is projected into GH in the detector plane. The atom-beam intensity is measured by the detector whose area is $4\Delta x\,\Delta z$ and which is capable of translation along the x and z directions by means of stepping motors.

Assume a uniform atom-number density $N_0(x',z')$ along the y' direction in the interaction region,[40] with the atom-number current density being

$$J_0'(x',z')=N_0(x',z')V . \tag{3}$$

The number of electrons scattered out of a volume element $dx'\,dy'\,dz'$ into solid angle $d\Omega$ per second is

$$di_s'(y',\theta,\phi)=\frac{J_0'(x',z')}{V} j_0(y')\sigma(\theta)d\Omega\,dx'\,dy'\,dz' , \tag{4}$$

where $j_0(y')$ is the electron-number current density (assumed to be uniform along the x' direction[41]) and $\sigma(\theta)$ is the cross section for a particular scattering process. In the present work we do not consider azimuthally asymmetric collisions; the analysis can be readily generalized to the case when dealing with state-selected beams.

The total number of electrons scattered out of $l\,dx'\,dz'$ into solid angle $d\Omega$ per second is then

$$di_s(\theta,\phi)=\int_{\text{over } l} di_s'(y',\theta,\phi)$$
$$=\frac{J_0'(x',z')}{V}\sigma(\theta)d\Omega\,dx'\,dz'\int_{\text{over } l} j_0(y')dy' . \tag{5}$$

The total electron number current i_0 is

$$i_0=h\int_{\text{over } l} j_0(y')dy' . \tag{6}$$

We can rewrite Eq. (5) as

$$di_s(\theta,\phi)=\frac{i_0}{hV}\sigma(\theta)d\Omega\,J_0'(x',z')dx'\,dz' . \tag{7}$$

Under the assumption of near-uniform atomic-beam density in the (x,z) and (x',z') planes, we can employ a simple scaling factor to relate differentials in interaction and detector regions:

$$h\,dx=H\,dx', \quad g\,dz=G\,dz' \tag{8}$$

so that

$$J_0'(x',z')dx'\,dz'=J_0(x,z)\frac{HG}{hg}dx'\,dz'$$
$$=J_0(x,z)dx\,dz , \tag{9}$$

where $J_0(x,z)$ is the atom-number current density in the detector plane. We can now write Eq. (7) as

$$di_s(\theta,\phi)=\frac{i_0}{hV}\sigma(\theta)d\Omega\,J_0(x,z)dx\,dz . \tag{10}$$

Since for each electron scattered at (θ,ϕ) one atom will be scattered from (x_1,z_1) to (x_2,z_2) in the detector plane, we can write

$$di_s(\theta,\phi)=dI(x_2-x_1,z_2-z_1) , \tag{11}$$

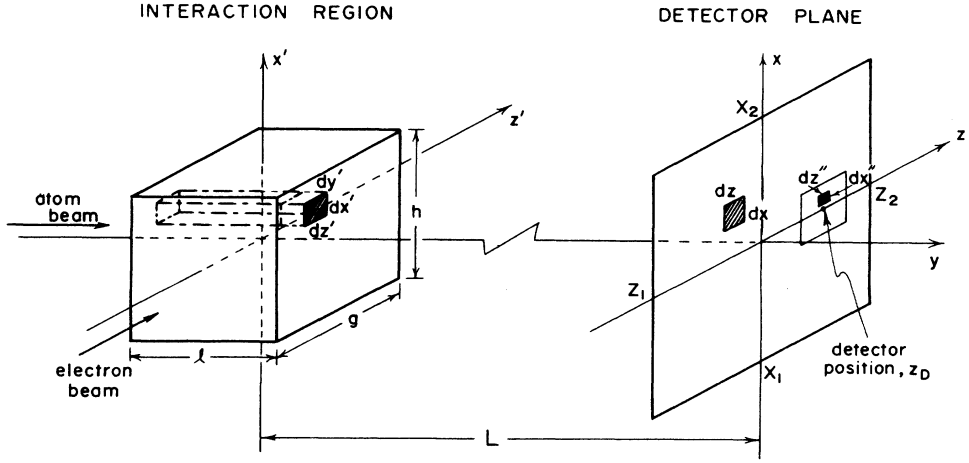

FIG. 1. Schematic diagram of the interaction and detection geometry. Detector height $2\Delta x$ and width $2\Delta z$ around z_D, $H=X_2-X_1$, $G=Z_2-Z_1$.

where $dI(x_2-x_1, z_2-z_1)$ is the number of atoms per second scattered from (x_1,z_1) into (x_2,z_2). The coordinates (x_2-x_1, z_2-z_1) in the recoil scattering space correspond to (θ,ϕ) in the electron scattering space by Eqs. (1) or (2). Thus

$$dI(x_2-x_1, z_2-z_1) = \frac{i_0}{hV}\sigma(\theta)\sin\theta\, d\theta\, d\phi\, J_0(x_1,z_1)dx_1\, dz_1 \ . \quad (12)$$

These relations relate the atom-number current density at a point (x_1,z_1) in the detector plane before scattering, the number of atoms scattered from that point to another point (x_2,z_2) corresponding to the scattering cross section $\sigma(\theta)$ and the electron number current i_0. It remains to connect Eq. (12) to the actual experimental data and to determine the appropriate limits of integration.

The scattering signal measured by an element of the detector $dx''\, dz''$ at x'',z'' can be written as

$$dI_s(x,z,\theta,\phi;x'',z'',\theta'',\phi'') = dI_{\rm in}(x,z,\theta,\phi) - dI_{\rm out}(x'',z'',\theta'',\phi'') \ , \quad (13)$$

where $x''-x$ and $z''-z$ are related to θ and ϕ by Eqs. (1) or (2). The scattering-in contribution from $dx\, dz$ at x,z to $dx''\, dz''$ at x'',z'' is

$$dI_{\rm in}(x,z,\theta,\phi) = dI_{\rm in}(x''-x,\, z''-z) = \frac{i_0}{hV}dx\, dz\, J_0(x,z)\sigma(\theta)\sin\theta\, d\theta\, d\phi \ . \quad (14)$$

The scattering-out contribution from dx'',dz'' at x'',z'' to the solid angle $d\Omega=\sin\theta''\, d\theta''\, d\phi''$ is

$$dI_{\rm out}(x'',z'',\theta'') = \frac{i_0}{hV}dx''\, dz''\, J_0(x'',z'')\sigma(\theta'') \times \sin\theta''\, d\theta''\, d\phi'' \ . \quad (15)$$

A. Differential cross section

The same detector is used to measure $I_0(z_D)$, the unscattered current at z_D, and $I_s(z_D)$, the corresponding scattered current. $I_s(z_D)$ is

$$I_s(z_D) = I_{\rm in}(z_D) - I_{\rm out}(z_D) \ . \quad (16)$$

In order to define $I_{\rm in}(z_D)$ and $I_{\rm out}(z_D)$ we have to include integration limits over the size of the detector and over the unscattered beam.

Also, note that for each polar scattering angle θ there are two azimuthal angles ϕ and $\pi-\phi$ which correspond to the same z. Electrons scattered at (θ,ϕ) and $(\theta,\pi-\phi)$ will both recoil atoms into the same point in the detector plane under the approximation $mv \ll MV$. Thus the principal contribution from the scattering process is described as

$$I^p_{\rm in}(z_D) = \frac{2i_0}{hV}\int_{X_1}^{X_2}dx\int_{Z_1}^{z_D-\Delta z}dz\, J_0(x,z)\int_{\theta(z_D-\Delta z-z)}^{\theta(z_D+\Delta z-z)}\sigma(\theta)\sin\theta\, d\theta\int_{\phi_1}^{\phi_2}d\phi \ , \quad (17)$$

$$\phi_1=\phi_2=0 \ \text{ if } \frac{\Delta x-x}{\alpha L\sin\theta}<-1 \text{ or } \frac{-\Delta x-x}{\alpha L\sin\theta}>1 \ , \quad (17a)$$

$$\phi_1 = \begin{cases} \sin^{-1}\dfrac{-\Delta x-x}{\alpha L\sin\theta} & \text{if } -1<\dfrac{-\Delta x-x}{\alpha L\sin\theta}\le 1 \\ -\dfrac{\pi}{2} & \text{if } \dfrac{-\Delta x-x}{\alpha L\sin\theta}\le -1 \ , \end{cases} \quad (17b)$$

$$\phi_2 = \begin{cases} \dfrac{\pi}{2} & \text{if } \dfrac{\Delta x-x}{\alpha L\sin\theta}\ge 1 \\ \sin^{-1}\dfrac{\Delta x-x}{\alpha L\sin\theta} & \text{if } -1<\dfrac{\Delta x-x}{\alpha L\sin\theta}<1 \ , \end{cases} \quad (17c)$$

and

$$I^p_{\rm out}(z_D) = \frac{i_0}{hV}\int_{-\Delta x}^{\Delta x}dx''\int_{z_D-\Delta z}^{z_D+\Delta z}dz''\, J_0(x'',z'')\int_{\theta(z_D+\Delta z-z'')}^{\pi}\sigma(\theta'')\sin\theta''\, d\theta''\int_0^{2\pi}d\phi'' \ . \quad (18)$$

See Fig. 1 for definitions of parameters.

The quantities x,z and θ,ϕ (or x'',z'' and θ'',ϕ'') are connected by Eqs. (1) for elastic and (2) for inelastic scattering.

Taking into account scattering events that occur in the region of the dc beam from X_1 to $-\Delta x$ and from Δx to X_2 across the detector area (Fig. 1), it is necessary to define correction terms $I^c_{\rm in}$ and $I^c_{\rm out}$ of this contribution to the $I_{\rm in}$ and $I_{\rm out}$, respectively. These are defined to be

$$I^c_{\rm in}(z_D) = \frac{2i_0}{hV}\left[\int_{X_1}^{-\Delta x}dx+\int_{\Delta x}^{X_2}dx\right]\int_{z_D-\Delta z}^{z_D+\Delta z}dz\, J_0(x,z)\int_0^{\theta(z_D+\Delta z-z)}\sigma(\theta)\sin\theta\, d\theta\int_{\phi_1}^{\phi_2}d\phi \quad (19)$$

and

$$I^c_{\text{out}}(z_D)=\frac{2i_0}{hV}\int_{-\Delta x}^{\Delta x}dx''\int_{z_D-\Delta z}^{z_D+\Delta z}dz''\,J_0(x'',z'')\int_0^{\theta(z_D-\Delta z-z'')}\sigma(\theta'')\sin\theta''\,d\theta''\left[\int_{\phi_1}^{\pi/2}d\phi''+\int_{-\pi/2}^{\phi_2}d\phi''\right] . \tag{20}$$

The correction terms are especially important for the scattering analysis in the shadow of the atomic beam. Thus Eq. (16) is

$$I_s(z_D)=I^p_{\text{in}}(z_D)+I^c_{\text{in}}(z_D)-I^p_{\text{out}}(z_D)-I^c_{\text{out}}(z_D) . \tag{21}$$

We will comment here on the influence of the atom velocity distribution on I_{in} and I_{out}. The atom-number current density in velocity interval dV in the interaction region is

$$\begin{aligned}dJ'_0(V,x',z')&=V\,dN_0(V,x',z')\\&=N_0(x',z')f(V)V\,dV ,\end{aligned} \tag{22}$$

where $N_0(x',z')$ and $f(V)$ are the atom-number density and the normalized atom speed distribution in the interaction region, respectively. The total number of atoms in the volume element $l\,dx'\,dz'$ in the dV interval is

$$l\,dx'\,dz'\,dN_0(V,x',z')=\frac{l}{V}dJ'_0(V,x',z')dx'\,dz' . \tag{23}$$

The corresponding number of electrons scattered into $d\Omega$ per second [cf. Eq. (7)] is

$$di_s(\theta,\phi)=\frac{i_0}{hV}\sigma(\theta)d\Omega\,dJ'_0(V,x',z')dx'\,dz' . \tag{24}$$

Then

$$\begin{aligned}J'_0(x',z')&=\int dJ'_0(V,x',z')\\&=N_0(x',z')\int f(V)V\,dV\\&=N_0(x',z')\bar{V} ,\end{aligned} \tag{25}$$

where $\bar{V}$ is the average atom speed.

Using Eq. (9), we can express atom-number current density in the detector plane through

$$\frac{dJ_0(V,x,z)}{V}=\frac{J_0(x,z)}{\bar{V}}f(V)dV . \tag{26}$$

Thus the scattering-in contribution can be written as

$$\begin{aligned}dI^p_{\text{in}}(V,z_D)&=\frac{2i_0}{h}\int dx\int dz\frac{dJ_0(V,x,z)}{V}\int\sigma(\theta)\sin\theta\,d\theta\int d\phi\\&=\frac{2i_0}{h}\int dx\int dz\frac{J_0(x,z)}{\bar{V}}f(V)dV\int\sigma(\theta)\sin\theta\,d\theta\int d\phi ,\end{aligned} \tag{27}$$

where the integration limits are the same as Eq. (17). Then we integrate over all velocities,

$$I^p_{\text{in}}(z_D)=\frac{2i_0}{h\bar{V}}\int_0^\infty f(V)dV\int dx\int dz\,J_0(x,z)\int\sigma(\theta)\sin\theta\,d\theta\int d\phi . \tag{28}$$

The scattering-out contribution is

$$I^p_{\text{out}}(z_D)=\frac{i_0}{h\bar{V}}\int_0^\infty f(V)dV\int dx''\int dz''\,J_0(x'',z'')\int\sigma(\theta'')\sin\theta''\,d\theta''\int d\phi'' . \tag{29}$$

The integration limits of Eqs. (28) and (29) are the same as the limits of Eqs. (17) and (18), respectively.

The correction terms for I^c_{in} and I^c_{out} should accordingly be rewritten, taking into account the velocity distribution. The integration limits will be then influenced by the x and z dependence of α (or β for inelastic scattering) which is a function of atomic beam velocity.

We derived expressions for all components of Eq. (21) assuming monoenergetic electrons. The actual electron energy distribution influences each component [Eqs. (17)–(20)] in two ways. First, $\sigma(\theta)$ is a function of electron energy. If we can assume that the cross section is a slowly varying function of energy over the energy distribution (i.e., potential scattering) then the nominal peak of that distribution is a good representation of the electron energy. This assumption, of course, will not hold in the case that the energy of the nominal peak corresponds to (or is very close to) resonant scattering of the observed process. A second influence is through the integration limits since α (or β for inelastic process) is a function of v. It has been shown[37] that this influence is negligible if $\delta E/4$ is much smaller than the electron energy after collision, where δE is the FWHM of the electron energy distribution. Since $\delta E\cong 0.5$ eV in the present experiment this condition is well satisfied. The above arguments are correct provided the observed process is well separated with respect to energy from other scattering channels. Both the energy and spatial resolving power have to be sufficiently high in order to avoid overlap of scattering signals from these different channels at a given detector position.

We now consider the influence of the experimental parameters to the computation of I_{in} and I_{out}. For simplicity, assume that elastic scattering is the only contributing process. We shall discuss the conditions under which differential cross sections can be determined from recoil scattering experiments, when this cannot be accomplished, and the conditions for which the validity of theoretical differential cross sections can be checked by modeling of scattering signals.

The unscattered beam current $I_0(z_D)$, measured along the x and z axes, serves to determine the integration limits X_1, X_2, Z_1, and Z_2. The scattered beam intensity $I_s(z_D)$ is measured along the z axis as a difference between atom current strengths when the electron beam is on and off:

$$I_s(z_D)=I_{\text{on}}-I_{\text{off}} . \tag{30}$$

Since I_s is two to four orders of magnitude smaller than I_0, experimental precautions must be taken to ensure linearity of the data. The electron number current i_0 is determined by measuring the current of all electrons that pass through the interaction region; this requires careful construction of the primary beam detector. The height of the interaction region h and the distance from that region to the detector plane L are geometrical parameters obtainable with good accuracy. The detector dimensions are 1×1 mm^2 and typical atomic beam profiles in the detector plane are 4×4 mm^2, around the center ($Z_1=-2$ mm, $Z_2=2$ mm). In the following discussion we consider the influence of beam and detector geometries on the analysis, starting first with the width of the detector. Since θ is not linearly dependent on z, left ($z_L=z_D-0.5$ mm) and right ends of the detector ($z_R=z_D+0.5$ mm) will detect atoms with different $\Delta\theta$ for different z_D, taking into account unscattered atoms that will reach a point $z=0$. In other words, we are for the moment neglecting the width of the atomic beam. We choose 5 and 20 eV, the two electron energies in this experiment, to calculate the range of θ for different positions of the detector. Results are shown in Table I for atomic species with different atomic masses and different average velocities during the experiment, namely, CsCl ($M=168$ amu, $\bar{V}=373$ m/s), LiBr ($M=87$ amu, $\bar{V}=527$ m/s), and Na ($M=23$ amu, $\bar{V}=1100$ m/s). Sodium is included in Table I for comparison with our past work; these values will be also used in a forthcoming paper which will report on electron scattering by laser-excited sodium.

A set of data showing angles at $z_D=0.5$ mm indicate that when the left edge of the detector can detect scattering-in at $\theta=0°$, a wide range of forward-scattered atoms ($\Delta\theta=5.5°$ up to 13.2°) can be seen by the detector. This implies that one cannot assume constant differential cross sections over the detector width, so that $\sigma(\theta)$ cannot be moved from the inside to the front of the integral in Eq. (17). This also means that it is not possible to determine differential cross sections from scattering data whenever the detector sees wide angular range of scattered atoms coming from the same point. These conditions exist so long as the detector is located within shadow of atomic beam or close to the right edge just outside of beam. In this case, one can model the scattered beam by calculating I_{in} and I_{out} using quantities of the present experimental setup and theoretically predicted differential cross sections.

The next two sets of data at $z_D=7.5$ mm and 15.0 mm show that the ranges of angles seen by the detector are from $\Delta\theta=1.0°$ to 2.6° and $\Delta\theta=0.7°$ to 1.9°, respectively. This angular resolution of the detector corresponds to scattering angles around 15° and 36° at $z_D=7.5$ mm and

TABLE I. Angular resolution as a function of detector and position.

Target	Electron energy (eV)	Detector width 1 mm, negligible beamwidth												Beamwidth 4 mm, negligible detector width									
		$z_D=0.5$ mm				$z_D=7.5$ mm				$z_D=15.0$ mm				$z_D=7.5$ mm					$z_D=15.0$ mm				
		θ_{zL}	θ_{zD}	θ_{zR}	$\Delta\theta$	θ_{zL}	θ_{zD}	θ_{zR}	$\Delta\theta$	θ_{zL}	θ_{zD}	θ_{zR}	$\Delta\theta$	θ_{BL}	θ_{BC}	θ_{BR}	$\Delta\theta$	θ_{BL}	θ_{BC}	θ_{BR}	$\Delta\theta$
CsCl	5	0	9.3	13.2	13.2	35.3	36.6	37.9	2.6	51.8	52.8	53.7	1.9	41.4	36.6	31.2	10.2	56.5	52.8	48.9	7.6
	20	0	6.7	9.5	9.5	25.2	26.1	27.0	1.8	36.6	37.2	37.9	1.3	29.4	26.1	22.3	7.1	39.7	37.2	34.6	5.1
LiBr	5	0	7.9	12.2	12.2	30.0	31.1	32.2	2.2	43.8	44.6	45.4	1.6	35.1	31.1	26.6	8.5	47.6	44.6	41.4	6.2
	20	0	5.6	7.9	7.9	21.1	21.9	22.6	1.5	30.6	31.1	31.7	1.1	24.7	21.2	18.7	6.0	33.2	31.1	28.9	4.3
Na	5	0	5.5	7.7	7.7	20.5	21.2	22.0	1.5	29.7	30.2	30.7	1.0	23.9	21.2	18.2	5.7	32.2	30.2	28.1	4.1
	20	0	3.9	5.5	5.5	14.5	15.0	15.5	1.0	20.9	21.2	21.6	0.7	16.9	15.0	12.8	4.1	22.6	21.2	19.8	2.8

around 21° and 53° at $z_D = 15$ mm. Under the assumption that differential cross sections are not changing rapidly away from $\theta = 0°$, $\sigma(\theta)$ can be removed from the third integral of Eq. (18) and assumed constant over the detector width.

We now consider the effect of the finite atom-beam width. We will analyze the set of angles corresponding to atoms scattered from the left edge (θ_{BL}), center (θ_{BC}), and right edge (θ_{BR}) of the atom beam onto the center of the detector. When $z_D = 7.5$ mm, the range of polar angles subtended by the beam width at z_D is from $\Delta\theta = 4.1°$ for Na at 20 eV ($12.8° < \theta < 16.9°$) to $\Delta\theta = 10.2°$ for CsCl at 5 eV ($31.2° < \theta < 41.4°$). For $z_D = 15.0$, these values are 2.8° ($19.8° < \theta < 22.6°$) to 7.6° ($48.9° < \theta < 56.5°$).

In summary, using our scattering analysis it is possible to analyze a region of measurements where one can extract differential cross sections from the scattering data and perform a full analysis of the measurements despite the limitations imposed by beam and detector widths. In the range of those detector positions where inelastically scattered atoms can be detected the same analysis can be performed using Eq. (2) to relate θ and z, taking into account the fact that the scattering signal is the sum of elastic and inelastic signals in the corresponding but different ranges of scattering angles.

B. Total cross section

Here we comment about another aspect of recoil analysis related to total σ_T and grand total σ_{GT} cross sections. Again, for simplicity assume that elastic scattering is the only contributing process. In this case $\sigma_T = \sigma_{GT}$. This is a good approximation for molecules where quasielastic scattering includes rotational and vibrational processes. For highly polar molecules, the electron excitation contribution to the total scattering for our energy range can be neglected.

Measurements performed inside the shadow of the dc beam are related to σ_T through the scattering-out contribution. The principal part of scattering out, defined by Eq. (18), can be written as the difference of two terms. By writing the θ'' integration in Eq. (18) as

$$\int_{\theta(z_D+\Delta z-z'')}^{\pi}\sigma(\theta'')\sin(\theta'')d\theta'' = \int_0^{\pi}\sigma(\theta'')\sin(\theta'')d\theta'' - \int_0^{\theta(z_D+\Delta z-z'')}\sigma(\theta'')\sin(\theta'')d\theta''$$
$$= \frac{1}{2\pi}\sigma_T - \int_0^{\theta(z_D+\Delta z-z'')}\sigma(\theta'')\sin(\theta'')d\theta'' , \tag{31}$$

we have

$$I^{p}_{\text{out}}(z_D) = \frac{i_0}{h\bar{V}} I_0(z_D)\sigma_T - I^{pc}_{\text{out}}(z_D) , \tag{32}$$

where

$$I_0(z_D) = \int_{-\Delta x}^{\Delta x} dx'' \int_{z_D-\Delta z}^{z_D+\Delta z} dz'' J_0(x'',z'') \tag{33}$$

and

$$I^{pc}_{\text{out}}(z_D) = \frac{2\pi i_0}{h\bar{V}} \int_{-\Delta x}^{\Delta x} dx'' \int_{z_D-\Delta z}^{z_D+\Delta z} dz'' J_0(x'',z'') \int_0^{\theta(z_D+\Delta z-z'')} \sigma(\theta'')\sin\theta''\, d\theta'' . \tag{34}$$

The first term contains σ_T and the second one we refer to as the principal correction term.

Combining Eqs. (21) and (32) (assuming $I_{\text{in}} = I^{p}_{\text{in}} + I^{c}_{\text{in}}$) one can define the total cross section as

$$\sigma_T = \frac{h\bar{V}}{i_0 I_0}(I_{\text{in}} - I^{c}_{\text{out}} - I_s + I^{pc}_{\text{out}}) . \tag{35}$$

All terms defined by Eqs. (17), (19), (20), (30), and (34), as well as I_0, correspond to the same detector position z_D.

The contribution of terms I_{in}, I^{c}_{out}, and I^{pc}_{out} to σ_T depends on the nature of the interaction and cannot be neglected *a priori* since all related equations include integration of $\sigma(\theta)\sin\theta$ over the detector width. From Table I it can be seen that, for the case of an effusive atom beam and geometrical parameters of the present experiment, integration over the detector width is from 0° to 13.2° or 9.5° for CsCl (5 and 20 eV). For LiBr the range is a little smaller, and for Na from 0° to 7.7° and 5.5° at 5 and 20 eV, respectively. Forward scattering is very strong for polar molecules; in Table II we show all contributions for LiBr and CsCl in order to compare our measured scattering intensities I_s with results obtained from model calculations and other experiments (see Sec. IV). It can be seen that because of the finite detector area the principal contribution to the scattering process, i.e., very small angle collisions, is unobservable as scattering-out, especially at low-impact energy. The scattering-in term is about 20% of I_s.

TABLE II. Contribution terms to σ_T in relative units at $z_D = 0$. The value of I_s is constant, $I_s = -1$.

Target	Electron energy (eV)	I_{in}	I^{pc}_{out}	I^{c}_{out}
LiBr	5	0.27	2.39	0.70
	20	0.18	1.57	0.55
CsCl	5	0.29	2.50	0.65
	20	0.20	1.61	0.59
Na	10	0.01	0.05	0.05

In the case of electron-*atom* scattering, inelastic processes can be as important as elastic scattering for σ_{GT}. Thus Eq. (35) will hold if Eqs. (17), (19), (20), and (34) are used separately for each involved transition and summed over all of them. So

$$I_{in} = \sum_i I_{in}^i , \tag{36}$$

$$I_{out}^c = \sum_i I_{out}^{c,i} , \tag{37}$$

$$I_{out}^{pc} = \sum_i I_{out}^{pc,i} . \tag{38}$$

Inelastically scattered electrons will recoil scattered atoms out of the dc beam if

$$\alpha L [1 - \sqrt{1 - (\Delta E/E)}] \geq G , \tag{39}$$

where G is the FWHM of the dc beam (4 mm in the present work), ΔE is the energy loss for the first inelastic process, and E the incident electron energy. Thus, the contributions from inelastic process Eqs. (36)–(38) will be zero. This is certainly the case for all alkali atoms, where only the elastic correction factors wil remain.

As an illustration, let us consider only resonant inelastic scattering of Na. One can write

$$I_s = I_{in}(3S) - I_{out}(3S + 3P) , \tag{40}$$

where

$$I_{out}(3S + 3P) = \frac{i_0 I_0}{h\bar{V}} [\sigma_T(3S) + \sigma_T(3P)] + I_{out}^c(3S) - I_{out}^{pc}(3S) . \tag{41}$$

Using Mitroy *et al.*[42] $3S$ and $3P$ data at 10 eV we have calculated all terms of Eq. (35) for Na and present them also in Table II. Here, the principal contribution term is I_s. Correction terms are of the order of 1%, compared to I_s. Similar results are obtained for 20 eV. We can conclude that for alkali atoms in the present energy range, the simplified equation[43]

$$\sigma_{GT} = \frac{h\bar{V}}{i_0 I_0} |I_s| , \tag{42}$$

as has been used in past work, is a good approximation for grand-total cross sections based on observable quantities. It will also hold for other species provided (a) Eq. (39) is satisfied, (b) the momentum transfer caused by electronic inelastic collisions is sufficient to result in complete scattering-out at all electron scattering angles, (c) elastic forward scattering is not as dominant as in highly polar molecules.

III. EXPERIMENT

The measurements reported here were performed on an apparatus which has been described in detail elsewhere.[36,39] Here we note only those apparatus parameters and characteristics appropriate to the present experiment.

The present paper is concerned exclusively with forward recoil scattering, for which the molecular scattering signal is measured in the shadow of unscattered molecular beam. In this region scattering-in contributions are dominated by small-angle scattering. The essential feature of small-angle-electron scattering by highly polar systems is its domination by the very long range inverse r^3 force (electron–point-dipole interaction); as a consequence one cannot fully resolve the angular distribution in the limit of very small angles. In the present work we show how one can instead employ a combination of data and model analyses to overcome this difficulty. In particular, we study electron scattering by one light molecule LiBr (87 amu) and one heavy molecule CsCl (186 amu) as a representative of highly polar systems.

The molecular beam was produced in a "quasieffusive" oven at a temperature of 1073 K for LiBr and 1043 K for CsCl. An oven nozzle is maintained at a temperature 60° higher to minimize the dimer concentration. The velocity distribution was not directly measured in this experiment. The relevant measured parameters which primarily determine the experimental velocity distribution are the nozzle temperature corresponding to vapor pressure of 4 and 6 torr in the oven for CsCl and LiBr, respectively. The thin-walled nozzle-throat aperture was approximately 0.25 mm in diameter. Using standard supersonic flow theory, we estimate the Knudsen number to be about 0.4 for both molecules, and using the empirical formula[44]

$$M = 1.2K^{(1-\gamma)/\gamma} \tag{43}$$

for the terminal Mach number M, where $\gamma = \frac{7}{5}$ for diatomic molecules, we obtain an estimate of the Mach number for both molecules to be 1.0. An estimation of the error in the absolute values of our final data resulting from uncertainty in M is $\pm 10\%$.

The spatial distribution of the molecular beam with and without scattering is monitored by a surface ionization detector which is capable of motion in two dimensions, in a plane ("detector plane") about 5 m downstream from the source. The (platinum) detector is a square, 1×1 mm^2. A magnetic mass spectrometer directs the surface-ionized ion beam to a high-current Channeltron electron multiplier (Galileo Electro Optics Corp. Model No. 4830) operating in the analog mode. (The alkali halides dissociate on the wire, so that we detect only the alkali ion constituent.) Channeltron operating voltages were less than 1100 V, so the gain was low enough to ensure linearity of the multiplier. The full unscattered beam is fed through a preamplifier directly to a high-sensitivity electrometer (Keithley, Model No. 642). The electron beam is square-wave modulated at 4 Hz; the resulting modulated scattering signal on the molecular beam is detected using a phase-sensitive lock-in amplifier (Ithaco Model No. 391A) whose output in turn is sampled by a Digital Equipment Corporation PDP11/03 computer programmed to act as a multichannel analyzer. At each detector position a data point is obtained as the average of approximately 1500 samples in 50 ms intervals (defined as a "run"). It is important to note that the unscattered (dc) and scattered (ac) beam intensities employ different measurement systems, and accordingly a calibration procedure is required to compare them so as to obtain absolute cross sections. This procedure is described at the end of this section.

The electron beam current is produced using an electron gun, previously described.[36,45] The current is uniformly distributed over an area defined by a length of 25.4 mm along the direction of the molecular beam and 0.8 mm in height. The molecular beam is defined by collimators to be slightly wider than the electron beam (1.18 mm) in order to ensure that all electrons pass through the molecular beam. The distance L between the end of the interaction region and the detector plane is 355 cm. The electron energy distribution, measured by a retarding potential technique, was 0.5 eV, FWHM. The electron energy in the interaction region is corrected for space charge and contact potential differences.[45]

Molecular beam profiles in vertical (x) and horizontal (z) directions (Fig. 2) are always recorded before each run, although variations in these are quite small over extended periods of time. The midpoints of the symmetric beam profiles are chosen as origin of coordinates ($x=0, z=0$). In the present work data is taken along the z axis at $x=0$, although the analysis presented in Sec. IV requires knowledge of the beam intensity in the x direction as well.

The present data are summarized in Table III. Each entry corresponds to a set of 3–7 runs, and average values after calibration are given in the table. The presented scattering signals correspond to an electron beam current of 4×10^{-4} A; their absolute values are three to four orders of magnitude smaller than the magnitude of the dc beam. At 20 eV, the electron current was 9.4×10^{-4} A. For consistency in presenting the data, we renormalized the scattering signal to the electron current that corresponds to 5 eV. The statistical error of each data point is within $\pm10\%$ of the average value. We estimate that the uncertainty of the position of the detector is less than 0.1 mm.

The calibration of scattered to unscattered beam signals is usually performed when the detector position is at the left edge of the dc beam, since at this position the scattering signal is very strongly dominated by scattering-out events. For a particular channeltron voltage the scattering signal output from the lock-in amplifier is converted into a current signal, which is then processed according to our standard data-taking protocol. For calibration purposes, the same signal from the channeltron is fed directly to the same electrometer used to monitor the dc beam and is compared to the dc beam using the standard analog-to-digital converter circuit of the control computer. The ratio of the lock-in signal to the scattering signal as measured using the electrometer serves as the calibration of the lock-in. We estimate that this procedure introduces an uncertainty in the absolute-cross-section determination of $\pm10\%$.

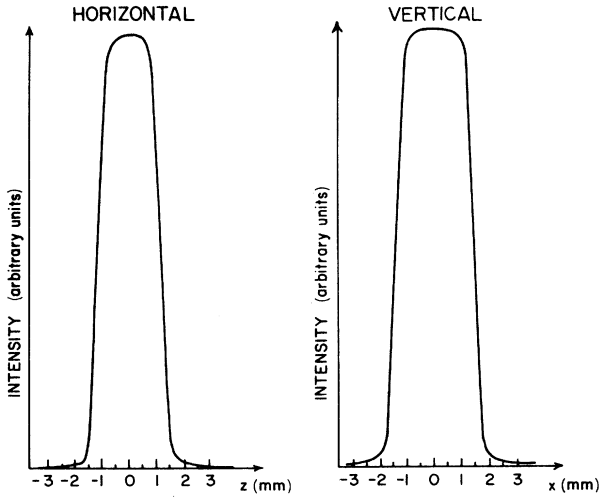

FIG. 2. Vertical and horizontal dc molecular-beam profiles.

Figures 3 and 4 are graphical presentations of experimental data for LiBr and CsCl, respectively. The figures show two sets of data each. The full unscattered molecular-beam profile in the detector plane is about 4 mm FWHM in both x,z directions for both molecules. The beam is essentially flat across its full width, with rather small tails at either side. The net scattering signals in the shadow of the dc beam are negative and asymmetric with respect to origin of coordinates, which is at the dc beam center. This asymmetry is attributable to competition between scattering-in (positive signal) versus scattering-out (negative signal), since scattering-in increases as the detector translates to the right, i.e., in the direction of momentum transfer, while scattering-out, normalized to the dc beam at the detector position, is in-

TABLE III. Unscattered (I_0) and scattered (I_s) molecular beam intensities in units of 10^{-11} A. Scattering intensities correspond to an electron beam current of 4×10^{-4} A.

Detector position z_D (mm)	CsCl I_0	CsCl I_s (units of 10^{-2}) 5 eV	CsCl I_s (units of 10^{-2}) 20 eV	LiBr I_0	LiBr I_s (units of 10^{-3}) 5 eV	LiBr I_s (units of 10^{-3}) 20 eV
−2.5	0.12	−0.97	−0.32	0.23	−4.16	−0.66
−2.0	0.66	−2.20	−0.73	1.00	−9.57	−2.77
−1.5	1.40	−3.00	−1.03	2.04	−16.10	−5.55
−1.0	1.67	−2.90	−1.01	2.42	−16.04	−5.84
−0.5	1.69	−2.86	−0.98	2.45	−14.81	−5.63
0.0	1.70	−2.60	−0.93	2.45	−14.55	−5.13
0.5	1.69	−2.42	−0.89	2.44	−13.39	−4.69
1.0	1.66	−1.85	−0.83	2.39	−11.89	−4.27
1.5	1.40	−1.02	−0.58	2.05	−8.27	−3.66
2.0	0.73	−0.43	−0.25	0.95	−1.41	−0.91
2.5	0.20	−0.01	−0.13	0.14	−0.06	−0.10

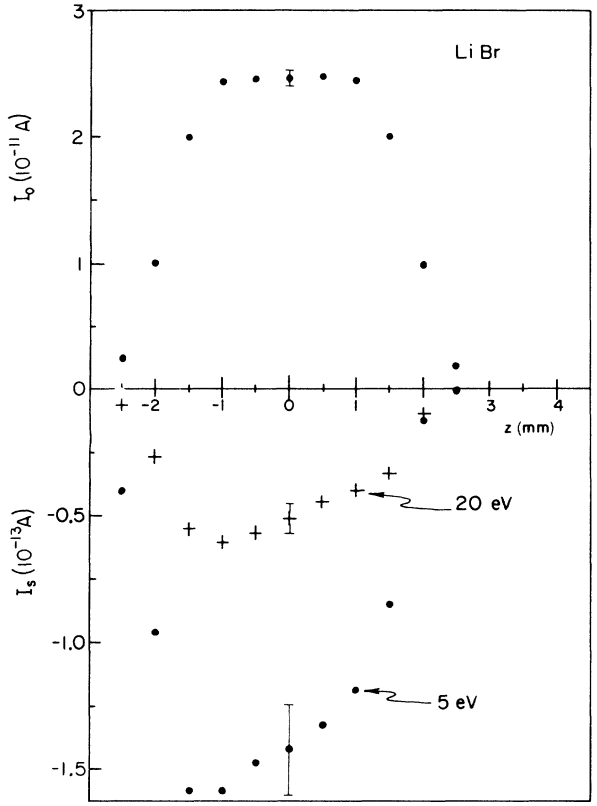

FIG. 3. Measured unscattered and scattered beam intensities of LiBr.

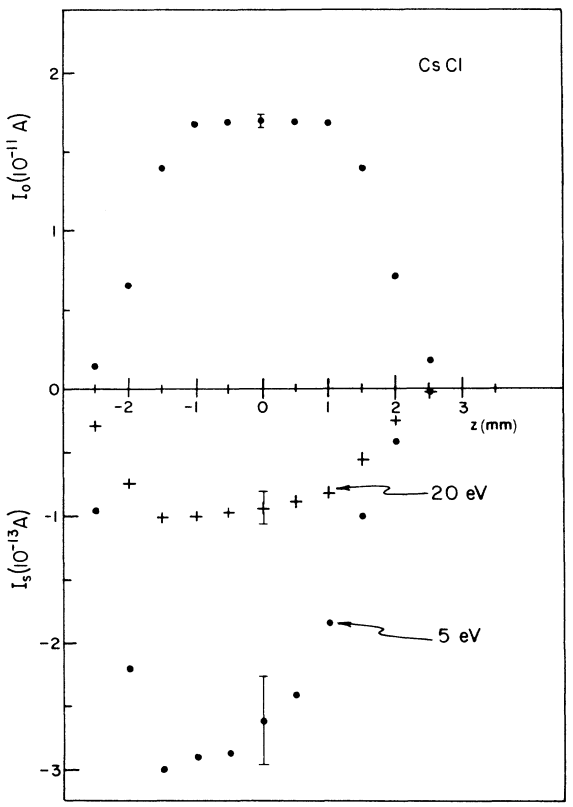

FIG. 4. Measured unscattered and scattered beam intensities of CsCl.

dependent of detector position. When the detector is sufficiently far to the right, the scattering signal will change sign, at the point where scattering-out from the residual beam equals the integrated contribution of scattering-in. Beyond this point the signal becomes positive, so that when the dc shadow is left behind one is observing scattering-in from a range of angles which depends on detector position, with no scattering-out contribution at all.

IV. ANALYSIS OF THE DATA

In Sec. II we performed a kinematic analysis of the recoil-scattering experiment. Here we employ this analysis in order to compare our scattering data with cross sections obtained from several theoretical models and calculations, as well as with existing experiments. The analysis is similar in principle to procedures used in extracting cross sections from transport data in weakly ionized plasmas via the Boltzmann collision integrals. In this latter case, one can start with trial cross sections and by a suitable iteration converge on the correct values (this assumes uniqueness, which applies at least in the case of elastic scattering below the first electronic inelastic threshold). In our case we could, in principle, also construct our cross sections uniquely by iteration systematically taking into account scattering-in at larger and larger angles, as one proceeds across the scattered beam from left to right. However, this procedure would require very precise data, particularly at small scattering angles; we reserve the performance of such an analysis for a later date. Here we employ a somewhat simpler strategy, by using several model energy- and angle-dependent cross sections, constructing scattering curves from them, and comparing with the actual scattering data. Also, as noted above, we compare our results using the kinematic analysis with existing experimental data.

For elastic scattering $\alpha=\beta$, and for rovibrational inelastic collisions $\alpha\cong\beta$, which we will refer to as quasielastic scattering. In the present case we need not be concerned with electronically inelastic collisions, which at the energies employed here are not observed within the dc beam shadow (e.g., for a 5-eV energy loss[29] at an electron energy of 20 eV the smallest molecular deflection, corresponding to 0° scattering, is 98 mm). In the analysis we deconvolute the observed undeflected molecular-beam shape to remove the effect of the finite detector width. The deconvoluted molecular beam possesses a nearly trapezoidal shape with the same half width (FWHM) as the measured one, 3.5 mm with a 3.0 mm plateau, symmetric about the beam center. We also consider in the analysis a deconvoluted vertical-beam profile which has the same shape as the horizontal one, but wider FWHM, as can be seen in Fig. 2. The principal experimental parameters used are

$$i_0=4\times10^{-4}\ \text{A}=2.5\times10^{15}\ \text{electrons/sec}\ ,$$

$$h=0.8\ \text{mm},\quad L=3.55\ \text{m},\quad \Delta x=\Delta z=0.5\ \text{mm}\ ,$$

$T=1133$ K for LiBr, and 1103 K for CsCl.

In the Appendix we demonstrate the application of this

model analysis to the simplified case of a rectangular molecular beam using the first Born approximation. The demonstration is useful to illustrate the recoil analysis, particularly to illustrate the competing roles played by scattering out (which is almost independent of detector position within the beam shadow), and scattering in, which increases monotonically as the detector translates in the direction of the electron-beam momentum. Here we apply the same analysis using the actual beam shape, employing Eq. (21) assuming a velocity as the average beam velocity with Mach number[46] 1.0.

The three models employed are the first Born approximation (BA), a semiclassical perturbation approximation by Dickinson[47] (SCP), both for the point dipole, computational results from a hybrid calculation (HYB) by Siegel *et al.*,[48] and an experimental comparison with the results of Vušković and Srivastava[29] (VS).

BA is averaged over all dipole orientations; this is equivalent to the rotating-point-dipole Born approximation

$$\sigma(\theta)=\frac{D^2}{6Ea_0\sin^2(\theta/2)} . \tag{44}$$

In the present calculation $\theta_{\min}=0.03°$. The choice of cutoff angle might be considered as critical because of the very strong forward scattering produced by the monopole-dipole interaction. However, this effect is somewhat mitigated by the solid-angle factor contributing to $\sigma(\theta)$. To estimate the importance of choosing a sufficiently small value for $\theta_{\min}$, we have made additional computations with values of $\theta_{\min}$ down to 0.002°. The results for I_s increased by about 3% at the smallest $\theta_{\min}$, ensuring that we have achieved reasonable convergence.

The SCP model was applied for moderately small and intermediate angles, between the θ_1 and θ_2, as[47]

$$\sigma(\theta)=\frac{\pi eD}{64E\sin^3(\theta/2)} , \tag{45}$$

where E is the electron energy and D is the molecular-dipole moment. In the low angular range BA is used up to θ_1, defined by

$$\frac{\sin\theta_1}{2}=\frac{3\pi ea_0}{32D} . \tag{46}$$

For CsCl and LiBr θ_1 equals 8.14° and 11.86°, respectively. Above θ_2, defined as

$$\theta_2=\begin{cases}60°, & E\le E_0\\ 2\sin^{-1}\left[\dfrac{(E_0/E)^{1/3}}{2}\right], & E\ge E_0 ,\end{cases} \tag{47}$$

where $E_0=\pi eD/2R_e^2$, and R_e is the internuclear separation, $\sigma(\theta_2)$ is assumed constant up to 180°.

The Siegel *et al.* hybrid S-matrix technique HYB (Ref. 49) incorporates the potential of the molecular core, the point dipole potential, and the first Born approximation. Their calculations are only available for CsCl.[48] These reproduce well the experimental elastic angular distributions of Vušković and Srivastava[29] at both 5 and 20 eV, when normalized at 30°. They demonstrated that the shoulder at around 30° is attributable to the strongly anisotropic molecular core. Thus they showed that *both* long- and short-range interactions make major contributions to scattering, even at relatively small scattering angles.

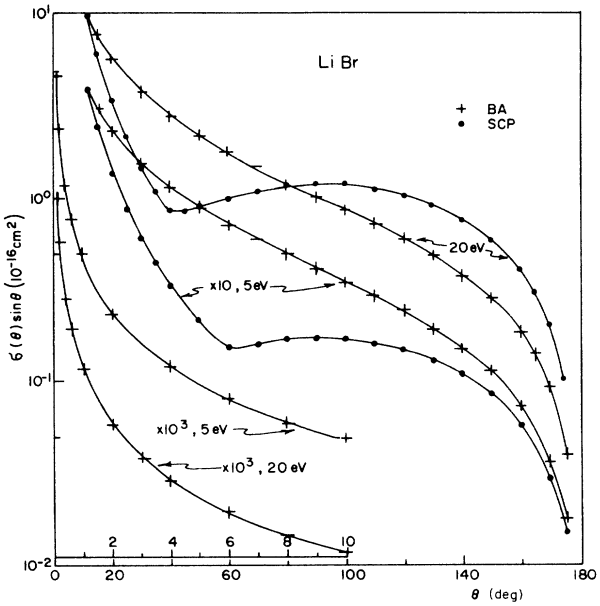

FIG. 5. Differential cross sections used in the calculations multiplied by $\sin\theta$. LiBr, 5 and 20 eV: +, BA and ●, SCP (Ref. 47). Inset BA (0°–10°) used by both approximations.

Experimental data at 5 and 20 eV, quasielastic, are available in the angular range 10° to 120° (VS). The VS normalization was made at 15° to HYB. This angle was chosen as the normalization point because the HYB calculations agreed well at 15° with SCP. In order to com-

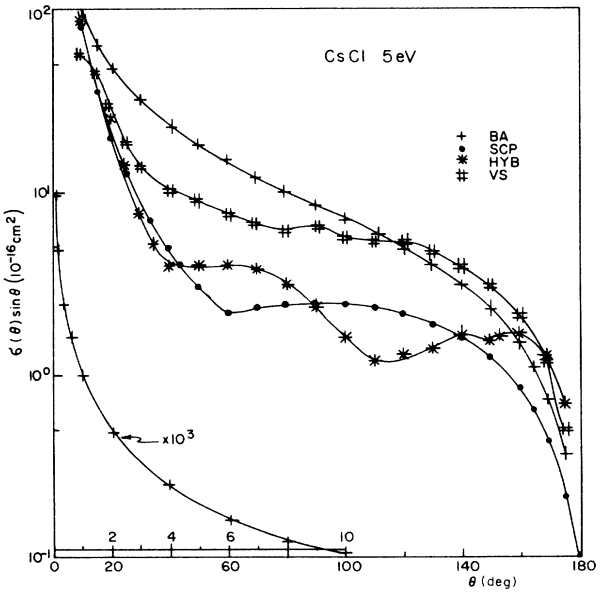

FIG. 6. Differential cross sections used in the calculations multiplied by $\sin\theta$. CsCl, 5 eV: +, BA; ●, SCP (Ref. 47); *, HYB (Ref. 48); and #, VS (Ref. 29). Inset BA (0°–10°) used by all approximations.

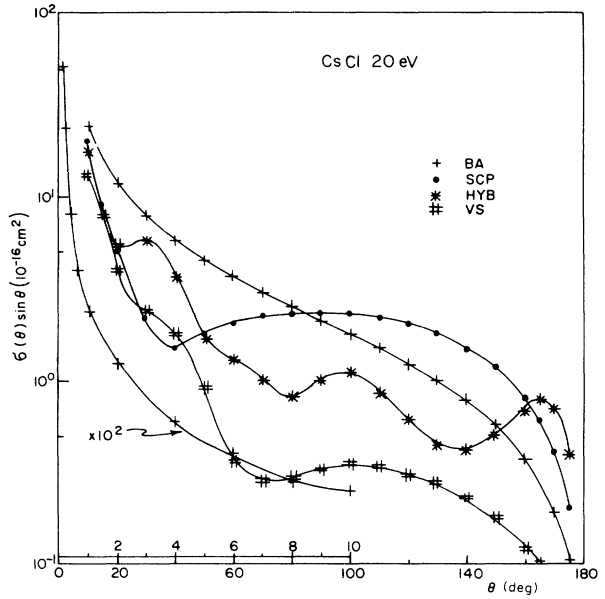

FIG. 7. Differential cross sections used in the calculations multiplied by $\sin\theta$. CsCl, 20 eV: +, BA; ●, SCP (Ref. 47); *, HYB (Ref. 48); and #, VS (Ref. 29). Inset BA (0°–10°) used by all approximations.

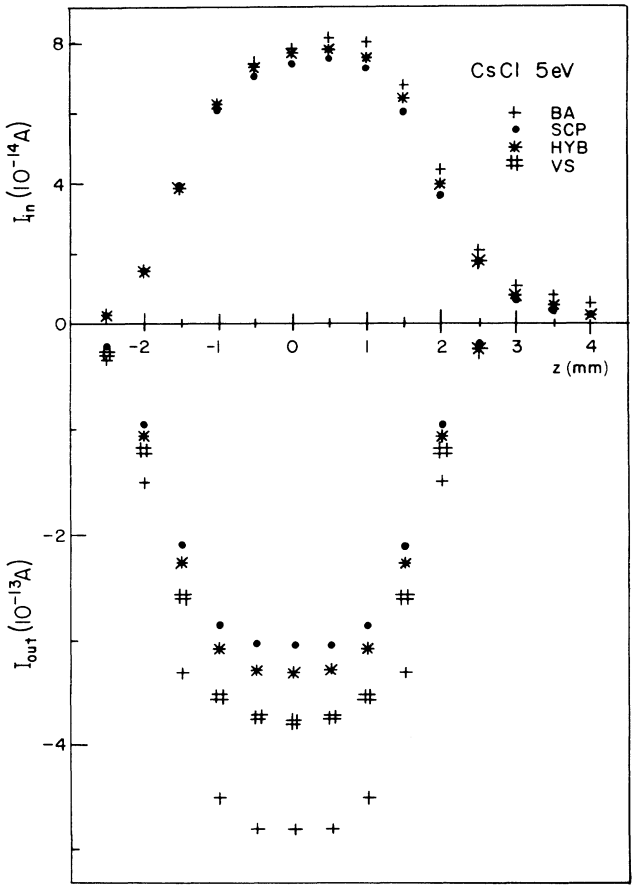

FIG. 8. Calculated I_{in} and I_{out} with measured unscattered beam for CsCl, 5 eV using $\sigma(\theta)$: +, BA; ●, SCP (Ref. 47); *, HYB (Ref. 48); and #, VS (Ref. 29).

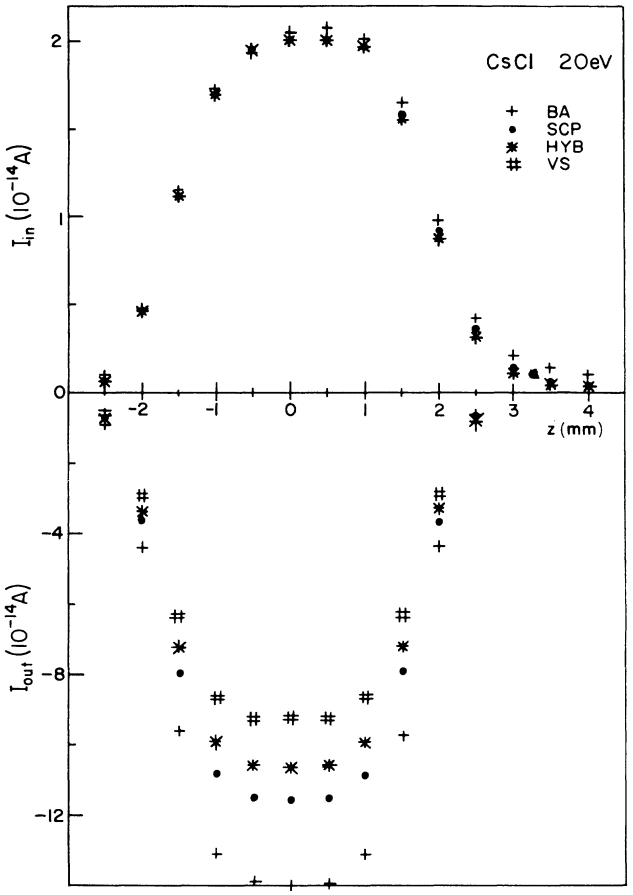

FIG. 9. Calculated I_{in} and I_{out} with measured unscattered beam for CsCl, 20 eV using $\sigma(\theta)$: +, BA; ●, SCP (Ref. 47); *, HYB (Ref. 48); and #, VS (Ref. 29).

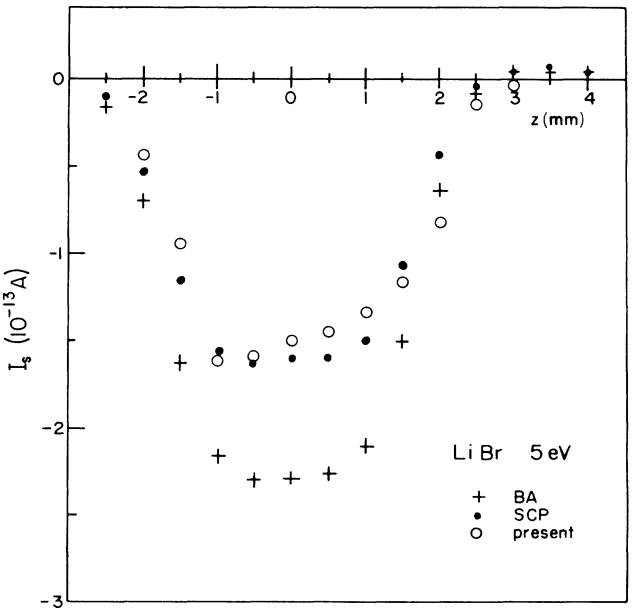

FIG. 10. LiBr scattering signal I_s at 5 eV: ○ present. Calculated using $\sigma(\theta)$: +, BA; and ●, SCP (Ref. 47).

pare these data with the present work it was necessary to extrapolate to very small angles. This was accomplished by joining the data to the BA calculation up to 8.14°, allowing for a linear extrapolation between BA at 8.14° and the VS data at 10°. The VS value of $\sigma(120°)$ is used as a constant up to 180°.

Since our analytic model employs integration of $\sigma(\theta)\sin\theta$ in different ranges of scattering-angle limits, we are presenting in Fig. 5 this quantity as a function of θ for 5 and 20 eV for LiBr using BA and SCP. Figures 6 (5 eV) and 7 (20 eV) show BA, SCP, HYB, and VS computations for CsCl. Figure 8 and 9 show calculated I_{in} and I_{out} for CsCl corresponding to the computations from Figs. 6 and 7, respectively. Results for LiBr are similar. Since all $\sigma(\theta)$ curves are the same in the small angular range (0°–8.14° for CsCl), because all models use the same BA for small angles, the I_{in} contribution to the scattering signal remains practically the same, regardless of the model employed. This is particularly true at 20 eV, at which energy electrons scattered above about 10° contribute little to I_{in}, although this statement is almost equally valid at 5 eV.

The contribution of I_{out} is indeed sensitive to scattering above 10°. Referring to Figs. 5–7 it can be seen that quantitative analysis must be employed to determine whether intermediate- or large-angle scattering dominate the total cross section. This in turn affects the scattering-out calculations through Eqs. (18) and (20).

The sum of I_{in} and I_{out} yields the observable I_s shown together with the present data in Figs. 10 and 11 for LiBr and Figs. 12 and 13 for CsCl at 5 and 20 eV, respectively. The fact that the present data agree within experimental error with SCP and HYB calculation means that the quasielastic total cross section calculated with SCP and HYB should both produce correct results. That also implies

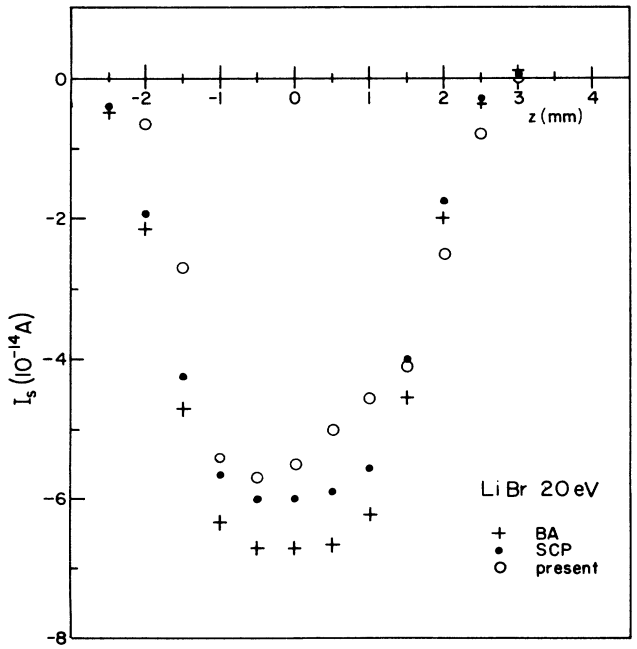

FIG. 11. LiBr scattering signal I_s at 20 eV: ○ present. Calculated using $\sigma(\theta)$: +, BA; and ●, SCP (Ref. 47).

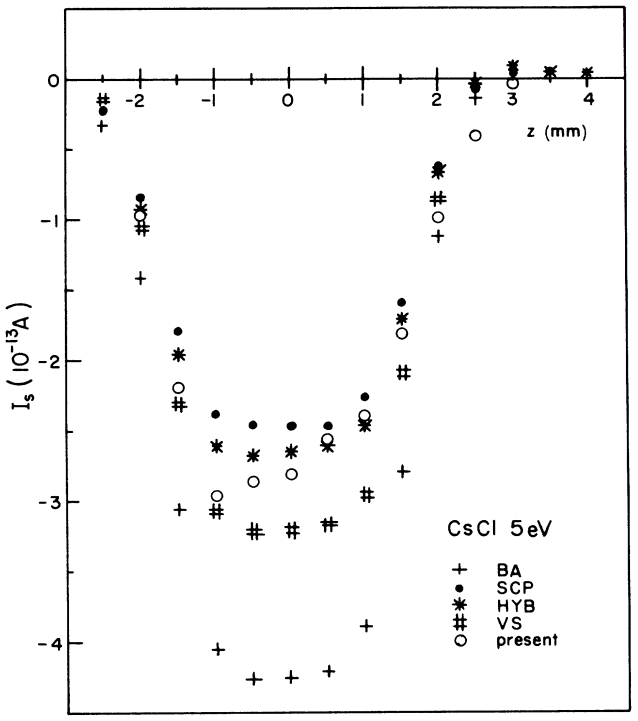

FIG. 12. CsCl scattering signal I_s at 5 eV: ○, present. Calculated using $\sigma(\theta)$: +, BA; ●, SCP (Ref. 47); *, HYB (Ref. 48); and #, VS (Ref. 29).

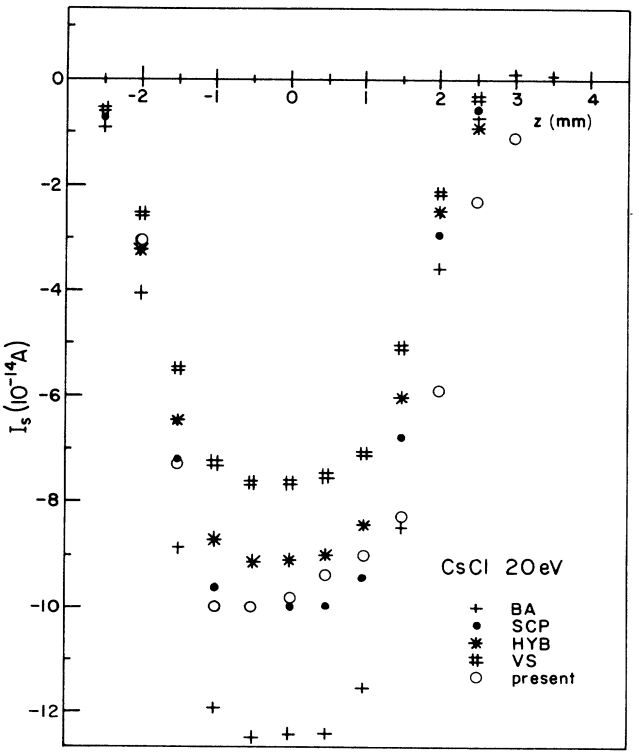

FIG. 13. CsCl scattering signal I_s at 20 eV: ○, present. Calculated using $\sigma(\theta)$: +, BA; ●, SCP (Ref. 47); *, HYB (Ref. 48); and #, VS (Ref. 29).

TABLE IV. Total cross sections σ_T (Å^2); included terms are indicated.

Target	Electron energy (eV)	I_s	I_s, I_{in}	$I_s, I_{in}, I^c_{out}, I^{pc}_{out}$
LiBr	5	118	149	350
	20	45	53	99
CsCl	5	233	298	729
	20	80	96	178

that there is no unique medium and large angular dependence of the $\sigma(\theta)$ curve, provided that the partial integral between θ_1 and π remains fixed.

The momentum transfer or diffusion cross section

$$\sigma_M = 2\pi \int_0^{\pi} \sigma(\theta)(1-\cos\theta)\sin\theta \, d\theta \tag{48}$$

and viscosity cross section

$$\sigma_V = 2\pi \int_0^{\pi} \sigma(\theta)\sin^3\theta \, d\theta \tag{49}$$

are more sensitive to the shape of the medium- and high-angle scattering $\sigma(\theta)$ curve.

Measured angular distributions of quasielastically scattered electrons by CsCl (VS), normalized at one point (15°) to HYB, as mentioned above, differ from the present data beyond experimental error. The angular distribution of intensity obtained in a conventional scattering experiment seems to be more reliable to normalize with respect to total cross section than to one point. Here we choose SCP to calculate partial σ_T (to avoid very small scattering angles) in the range of θ where the VS measurements were performed, and we renormalize the VS data to these values. A factor of 0.62 is applied at 5 eV and 1.92 at 20 eV, and we refer now to the renormalized data as VS*. Calculated I_s using VS* produce the same results as SCP. This is additional indication that I_s is not sensitive to the shape of $\sigma(\theta)$ curve. We believe that VS* should yield realistic values for the transport cross sections σ_M and σ_V.

We also calculated σ_T from the present data employing Eq. (35), since all nonobservable contributing terms require calculation of $\sigma(\theta)$ up to approximately 10° below which BA is a good approximation. The smallest scattering angle $\theta_{min}=0.03°$ is the same as before. As stated above all calculated terms change by about 3%, as does I_s, when θ_{min} is reduced to 0.002°. At the same time, σ_T is extremely sensitive to all contributing terms included in Eq. (35). From Table IV one can see that σ_T is two–three times larger than those values obtained when only measured quantities are taken into account.

Based on BA, SCP, HYB, and VS* $\sigma(\theta)$ curves, we calculated σ_T. As is mentioned above, all such curves use BA for the small-angle range. In this calculation σ_T is very sensitive to θ_{min}; it changes by about 40% when the θ_{min} is decreased from 0.03° to 0.0002°. Although convergence is not achieved, we calculate σ_T down to 0.03° since the present data are not sensitive below 0.03°. We also calculate σ_M and σ_V with all $\sigma(\theta)$ curves employing Eqs. (48) and (49), respectively.

In Table V we present σ_T, σ_M, and σ_V for both LiBr and CsCl molecules at electron energies 5 and 20 eV calculated from BA, SCP, HYB, VS* together with Becker *et al.*[33] (BFSS) experimental data and the present data. We estimate the error in our present σ_T to be ±20%, attributable mainly to statistical errors, uncertainty in the calibration of the scattered beam intensity with respect to the dc beam, and the error in evaluation of the velocity distribution of the atom beam. We also believe that the error in σ_M of VS* is ±30%, due to the statistical error in determining the angular distribution of the VS data, to

TABLE V. Total, σ_T; momentum transfer, σ_M; viscosity, σ_V cross sections. $\theta_1=11.68°$ for LiBr and 8.14° for CsCl.

Target	Electron energy (eV)	Model	σ_T (Å^2)			σ_M (Å^2)			σ_V (Å^2)		
			$0-\theta_1$	$\theta_1-\pi$	$0-\pi$	$0-\theta_1$	$\theta_1-\pi$	$0-\pi$	$0-\theta_1$	$\theta_1-\pi$	$0-\pi$
LiBr	5	BA	342	116	458	0.5	51.0	51.5	1.1	50.4	51.5
		SCP	342	57	399	0.5	24.2	24.7	1.1	19.6	20.7
		pres.			350						
	20	BA	86	29	115	0.1	12.8	12.9	0.3	12.6	12.9
		SCP	86	21	107	0.1	15.2	15.3	0.3	10.7	11.0
		pres.			99						
CsCl	5	BA	673	276	949	0.5	106.1	106.6	1.1	105.6	106.7
		SCP	673	111	784	0.5	35.9	36.4	1.1	29.6	30.7
		HYB	673	131	804	0.5	38.7	39.2	1.1	31.5	32.6
		VS*	673	111	784	0.5	61.2	61.6	1.1	48.9	50.0
		BFSS			680			20.0			
		pres.			729						
	20	BA	168	69	273	0.1	26.6	26.7	0.3	26.4	26.7
		SCP	168	46	214	0.1	30.1	30.2	0.3	20.8	26.1
		HYB	168	40	208	0.1	15.9	16.0	0.3	12.7	13.0
		VS*	168	46	214	0.1	10.8	10.9	0.3	10.3	10.8
		BFSS[a]			400			50.0			
		pres.			178						

[a]Results at 16 eV.

the estimation of the differential cross sections above 120°, and to the difference between the present I_s and the I_s calculated using SCP, that served as the recalibration of the VS curve. The estimated error in the VS* σ_V values are somewhat smaller.

From the table one can see that the present data are somewhat smaller than all theoretical results. The agreement is up to 20% for SCP and HYB, while BA differ more than these, exceeding 50% at 20 eV for CsCl. The difference between BFSS and the present data is not consistent since the present data are larger by 7% at 5 eV and smaller by more than a factor of 2 at 20 eV. (Note that the BFSS measurements were actually made at 16 eV.)

We believe that the most reliable values for σ_M (available only for CsCl) are those of VS*. The best agreement to σ_M, VS* are the HYB data, differing by about 50% below VS* at 5 eV and about 50% above VS* at 20 eV. Two other theories, BA and SCP, exceed that limit, with a difference of about a factor of 2 at 20 eV. The largest discrepancies compared to VS* are the experimental BFSS data, which are 2.5 times smaller at 5 eV and about 5 times larger than 20 eV VS* data. The fact the BFSS are at 16 rather than 20 eV cannot explain such difference. The viscosity cross sections σ_V obtained with VS* are more reliable than σ_M because the important scattering angles for this quantity were observed. Nevertheless, agreement with HYB data are within 50%.

V. CONCLUSION

The research presented in this paper addresses problems associated with elastic scattering, particularly though not exclusively concerned with very small angles, that deal with various aspects of the role played by angular resolution. Such problems are present in conventional as well as recoil types of crossed-beam experiments. The present work, which deals with low-energy scattering by alkali-halide molecules, in which the monopole-dipole interaction plays such an important role, is particularly sensitive to very-small-angle collisions. We have shown how to take such collisions into account when attempting to affect comparison of experiment with calculation, even though such small-angle interactions are not observable because of the finite apertures, beam widths, etc. of any crossed-beam experiment. One (not surprising) consequence of our analyses is that BA is valid in the small-angle range down to about 0.03°. This is a consequence of the fact that, taken in conjunction with medium- and large-angle scattering obtained by SCP and HYB, the calculated scattering signals reproduce our measurements in both relative shape and, most importantly, in absolute values reasonably well. We have also indicated, based on our model analysis, under what conditions absolute total cross sections can be obtained from recoil-technique measurements.

With regard to conventional scattering experiments, we also note from this work that calibration of measured electron scattering current intensities in order to obtain absolute values is better done over a range of angles where both experimental and theoretical $\sigma(\theta)$ curves are well determined, using a partial integral cross section, rather than at a single point, as is generally the custom. This is because a relatively small error in such a single-point calibration can propagate nonlinearly, as one moves further away from the single calibration angle. This is especially important in the present energy range where $\sigma(\theta)$ is needed to obtain momentum-transfer cross sections for which no direct measurements exist.

Our final results, and comparisons with existing theoretical and experimental results, are summarized in Figs. 10–13 and in Table V. Our measured scattering signals shown in the figures as reproduced using SCP and HYB models indicated the need to renormalize the VS data. This in turn yields momentum-transfer cross sections that differ significantly from the BSFF measurement. The present integral cross sections agree to within 20% with calculated ones using SCP and HYB that employ BA from about 10° down to 0.03°.

ACKNOWLEDGMENTS

We are grateful to Dr. Bernardo Jaduszliwer for his invaluable contributions to the design and construction of the experimental apparatus and for his continued help with the data analysis. We thank Dr. Thomas M. Miller for a careful reading of the manuscript. We are also pleased to acknowledge the assistance of Mr. Tong-yin Jiang during the latter phases of the experiment. This work was supported in part by the U.S. Department of Energy (Division of Chemical Sciences, Office of Basic Energy Sciences) and by the National Science Foundation.

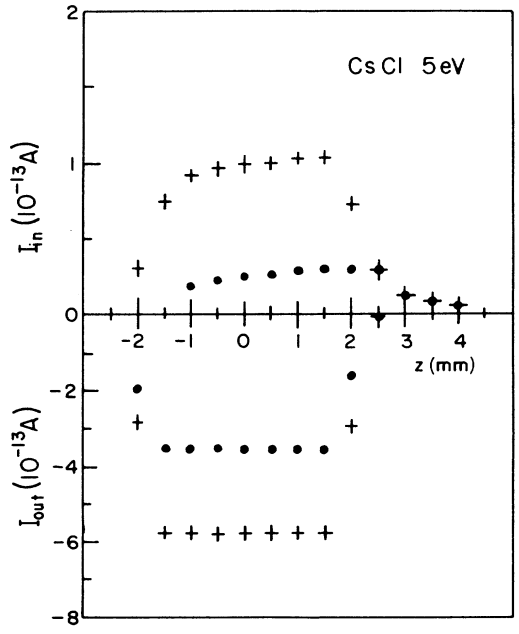

FIG. 14. Scattering-in and scattering-out calculated for CsCl, 5 eV using $\sigma(\theta)$ BA: ●, I^p_{in} and I^p_{out}; +, I^p_{in} with I^c_{in} and I^p_{out} with I^c_{out}.

APPENDIX: APPLICATION OF ANALYTIC MODEL TO RECTANGULAR MOLECULAR BEAM

Here we demonstrate how I_{in} and I_{out} contribute to the scattering signal in the shadow of the unscattered beam and in its vicinity. As a model differential cross section we employ the first Born approximation for 5 eV electrons scattered by CsCl. We assume a simplified square dc beam 4×4 mm^2 in the detector plane, possessing the same intensity as is measured at the center of the experimental beam. We assume that the molecular beam is effusive with a Maxwellian velocity distribution that can be defined by the temperature of the oven. In this case the average velocity can be calculated by $\bar{V}=(8kT/\pi M)^{1/2}$. Figure 14 shows I_{in} and I_{out} versus detector position, calculated using $\bar{V}$. The points are calculated using Eqs. (17) and (18), respectively, and crosses are calculated with correction terms as well [Eqs. (17) and (19) for I_{in} and (18) and (20) for I_{out}].

Equation (17) completely describes I_{in} outside of the shadow of the dc beam. In this region I_{out} is zero. However, inside of the dc beam shadow, the correction term contributions are very important.

Results calculated using Eq. (17) alone possess nonzero amplitudes for I_{in}^{p} only when the molecular beam has a component to the left of the detector. In the present example, molecules contributing to the first nonzero point correspond to electron collisions that are scattered between 0° and 9.3° (polar scattering angle). By moving the detector along the electron momentum direction (i.e., to the right) I_{in}^{p} rises very slowly due to increasing contributions of large-angle scattering. The maximum value of I_{in}^{p} occurs when the detector is located just outside the dc beam, since the largest range of polar scattering angles occurs at that detector position. The slope of the I_{out}^{p} curve [Eq. (18)] is a mirror image of the dc beam except for the first and last points (where half the detector is exposed to the beam).

When the correction term [Eq. (20)] is included in the calculation the amplitude of I_{out} increases by about 50% (the slope remains the same) because molecules scattered out of the detector corresponding to different azimuthal angles for the same small polar angle are taken into account. The correction term [Eq. (19)] actually dominates I_{in}, its amplitude being changed by a factor of about 4 or 5. Also, the shape of the curve is changed. This is because small-angle scattering into the detector from the portion of the dc beam that is located above and below the detector is included in the calculation. The amplitude of I_{in} is already 30% of its maximum value when half the detector is exposed to the dc beam (on the left side of the beam). When the detector is fully inside of the beam ($z_D=-1.5$ mm), the amplitude rises to about 75%, even though the first term contribution is still zero.

We have also calculated I_{in} and I_{out} curves with a full Maxwellian velocity distribution of molecules (rather than simply $\bar{V}$). The results differ in magnitude only by about 2% compared to the $\bar{V}$ calculations.

---

*Permanent address: Institute of Physics, P.O. Box 57, 11001 Belgrade, Yugoslavia.

†Present address: School of Physical Sciences, The Flinders University of South Australia, Bedford Park, South Australia 5042, Australia.

‡Present address: Department of Physics, University of Idaho, Moscow, ID 83843.

[1]H. S. W. Massey, Proc. Cambridge Philos. Soc. **28**, 99 (1932).

[2]D. W. Norcross and L. A. Collins, in *Advances in Atomic and Molecular Physics,* edited by D. R. Bates and B. Bederson (Academic, New York, 1982), Vol. 18, pp. 341–397.

[3]Y. Itikawa, Phys. Rev. **46**, 117 (1978).

[4]N. F. Lane, Rev. Mod. Phys. **52**, 29 (1980).

[5]N. T. Padial, D. W. Norcross, and L. A. Collins, Phys. Rev. A **27**, 141 (1983).

[6]N. T. Padial and D. W. Norcross, Phys. Rev. A **29**, 1590 (1984).

[7]D. Teillet-Billy and J. P. Gauyacq, J. Phys. B **17**, 4041 (1984).

[8]T. F. O'Malley, L. Spruch, and L. Rosenberg, J. Math. Phys. **2**, 491 (1961).

[9]W. Domcke and C. Mundel, J. Phys. B **18**, 4491 (1985).

[10]W. Domcke and L. S. Cederbaum, J. Phys. B **14**, 149 (1981).

[11]R. Bijker and R. D. Amado, Phys. Rev. A **34**, 71 (1986).

[12]K. Jung, Th. Antoni, R. Muller, K. H. Kochem, and H. Ehrhardt, J. Phys. B **15**, 3535 (1982).

[13]R. F. Wallis, R. Hermann, and H. W. Milnes, J. Mol. Spectrosc. **4**, 51 (1960).

[14]K. Rohr and F. Linder, J. Phys. B **9**, 2521 (1976).

[15]K. Rohr and F. Linder, J. Phys. B **8**, L200 (1975).

[16]G. Seng and F. Linder, J. Phys. B **9**, 2539 (1976).

[17]K. Rohr, J. Phys. B **10**, L399 (1977).

[18]K. Rohr, J. Phys. B **11**, 1849 (1978).

[19]K. Rohr, J. Phys. B **11**, 4109 (1978).

[20]W. Sohn, K. H. Kochem, K. M. Scheuerlein, K. Jung, and H. Ehrhardt, J. Phys. B **20**, 3217 (1987).

[21]R. Azria, Y. Le Coat, and J. P. Guillotin, J. Phys. B **13**, L505 (1980).

[22]R. Azria, Y. Le Coat, D. Simon, and M. Tronc, J. Phys. B **13**, 1909 (1980).

[23]W. Sohn, K. Jung, and H. Ehrhardt, J. Phys. B **16**, 891 (1983).

[24]C. Schermann, I. Čadež, P. Delon, M. Tronc, and R. I. Hall, J. Phys. E **11**, 746 (1978).

[25]R. I. Hall, I. Čadež, C. Schermann, and M. Tronc, Phys. Rev. A **15**, 599 (1977).

[26]M. R. H. Rudge, S. Trajmar, and W. Williams, Phys. Rev. A **13**, 2074 (1976).

[27]S. K. Srivastava, H. Tanaka, and A. Chutjian, J. Chem. Phys. **69**, 1493 (1978).

[28]L. Vušković, S. K. Srivastava, and S. Trajmar, J. Phys. B **11**, 1643 (1978).

[29]L. Vušković and S. K. Srivastava, J. Phys. B **14**, 2677 (1981).

[30]M. G. Fickes and R. C. Stern, J. Chem. Phys. **60**, 4710 (1974).

[31]R. C. Slater, M. G. Fickes, W. G. Becker, and R. C. Stern, J. Chem. Phys. **60**, 4697 (1974).

[32]R. C. Slater, M. G. Fickes, W. G. Becker, and R. C. Stern, J. Chem. Phys. **61**, 2290 (1974).

[33]W. G. Becker, M. G. Fickes, R. C. Slater, and R. C. Stern, J. Chem. Phys. **61**, 2283 (1974).

[34]L. A. Collins and D. W. Norcross, Phys. Rev. A **18**, 467 (1978).

[35]B. Jaduszliwer, A. Tino, P. Weiss, and B. Bederson, Phys. Rev. Lett. **51**, 1644 (1983).

[36]B. Jaduszliwer, A. Tino, and B. Bederson, Phys. Rev. A **30**, 1269 (1984).

[37]A thorough one-dimensional analysis was presented by Stern and collaborators (Refs. 30–33); however, this analysis did not address problems associated with very-small-angle scattering, which is critical because of the finite detector dimensions.

[38]There is a complete literature on such analyses concerned with atom-atom (or molecule) as opposed to *electron*-atom (or molecule) collisions. See, for example, J. Baudon, in *Atomic Physics 11, Book of Invited Papers,* Proceedings of the 11th International Conference on Atomic Physics, Paris, 1988 (in press).

[39]B. Jaduszliwer, P. Weiss, A. Tino, and B. Bederson, Phys. Rev. A **30**, 1255 (1984).

[40]The atomic beam in the interaction region is defined by a collimator that subtends a solid angle of 5×10^{-7} rad with respect to the source and can therefore be safely assumed to possess uniform spatial flux density.

[41]Due to space charge within the electron beam produced by the oxide cathode, one can expect uniform electron beam current along the x' direction ($h=0.8$ mm) entering the interaction region. This is proved by near constant I_s signal along the vertical direction.

[42]J. Mitroy, I. E. McCarthy, and A. T. Stelbovics, J. Phys. B **20**, 4827 (1987).

[43]B. Bederson and L. J. Kieffer, Rev. Mod. Phys. **43**, 601 (1973).

[44]J. B. Anderson, R. P. Andres, and J. B. Fenn, Adv. Chem. Phys. **10**, 275 (1966).

[45]R. E. Collins, B. B. Aubery, P. N. Eisner, and R. J. Celotta, Rev. Sci. Instrum. **41**, 1403 (1970).

[46]A. Kantrowitz and J. Grey, Rev. Sci. Instrum. **22**, 328 (1951).

[47]A. S. Dickinson, J. Phys. B **5**, 967 (1977).

[48]J. Seigel, J. L. Dehmer, and D. Dill, J. Phys. B **14**, L441 (1981).

[49]J. Seigel, J. L. Dehmer, and D. Dill, Phys. Rev. A **23**, 632 (1981).